

through sediment pore waters. This admittedly far-fetched scheme requires all of the Au deposited in ejecta over at least 30 cm<sup>2</sup> of the ocean floor to have diffused into this 2.5-mm particle. There is evidence for chemical diffusion at least on a millimetre-scale. The clays surrounding the meteorite are light brown because they lack the hydrogenous manganese oxides that are ubiquitous in pelagic clays and which give them their dark-brown colour. During diagenetic alteration of metal and sulphides within the meteorite, a zone of reducing conditions in the surrounding sediments must have developed, reducing Mn to the soluble Mn<sup>2+</sup> (ref. 15) which could then diffuse outwards. Glauconite, which we infer to be a principal clay mineral in the altered meteorite, is also known to form only under reducing conditions<sup>16</sup>.

The Ir anomaly in DSDP Hole 576 was smeared across at least 30 cm by bioturbation<sup>7</sup>. In such slowly accumulating clays<sup>5</sup> this interval could represent as much as 0.5 Myr of sedimentation, so it is impossible to state with certainty that this object accreted at the same moment as the K/T projectile. Interplanetary dust from the asteroid belt is an unlikely source because it should be strongly biased against particles this large which are destroyed by collisions before solar wind induced drag can decelerate them into Earth-crossing orbits<sup>17</sup>. In any case, over 0.5 Myr, only ~2 × 10<sup>16</sup> g of interplanetary dust should accrete to the Earth, an amount which is <4% of the mass of the 10-km chondritic asteroid proposed for the K/T boundary<sup>1</sup>. Dust produced by a significant comet shower<sup>18</sup> is a potential source, but there is no independent physical evidence that such an event occurred 65 Myr ago. The K/T projectile itself is capable of producing unmelted meteorite fragments and should be considered the most plausible source. Numerical simulations of the Chicxulub impact show that vertical impact of a 10-km projectile at asteroidal velocities could result in as much as 10% of the projectile experiencing shock pressures below the melting point<sup>4</sup>. At more typical angles approaching 45°, even more material could survive. This has also been demonstrated in laboratory experiments of oblique impacts<sup>19</sup>, which have been discussed as the possible cause of asymmetries in the Chicxulub crater<sup>20</sup>. Also, a late Pliocene hypervelocity impact is known to have produced millimetre- to centimetre-sized unmelted meteorites<sup>21</sup> so the potential for meteorite survival is an established fact.

The fossil meteorite described in this study is, to our knowledge, the first K/T boundary sample with sufficient information from textural and chemical data to make inferences concerning its origin. Shuryatz *et al.*<sup>22</sup> reported micrometre-sized Ir nuggets in impact melt rocks from Chicxulub, and speculated that they might be derived directly from the projectile. Robin *et al.*<sup>23</sup> reported ~250-µm spheroidal debris with chondritic Ir concentrations and shapes reminiscent of partially melted interplanetary dust. These were in K/T sediments from DSDP Site 577, only 500 km west of Site 576. They made no specific interpretation of the source materials, other than that they were chondritic. The fossil meteorite from DSDP Hole 576 appears to be from (1) a chondritic meteorite with (2) significant amounts of metal and sulphide (4–8%), (3) large inclusions (>200 µm) of mafic minerals that also contained metal, and (4) 30–60% fine-grained matrix. The known meteorite groups that best fit these criteria could be the CV, CO and CR carbonaceous chondrites<sup>24–26</sup>. Type CM carbonaceous chondrites are possible, but they typically contain only 1–3% opaque minerals<sup>27</sup>. Unequilibrated ordinary chondrites are a less likely source because they have only 15% fine-grained matrix<sup>28</sup>. Carbonaceous chondrites constitute only a few per cent of observed meteorite falls<sup>29</sup>, but they may be an important component of the asteroid belt, as most of the Antarctic micrometeorites have characteristics typical of CM and CR chondrites<sup>30</sup>. □

Received 2 June; accepted 17 September 1998.

- Alvarez, L. W., Alvarez, W., Asaro, F. & Michel, H. V. Extraterrestrial cause for the Cretaceous-Tertiary extinction. *Science* **208**, 1095–1108 (1980).
- Hildebrand, A. R. *et al.* Chicxulub crater: A possible Cretaceous/Tertiary boundary impact crater on

the Yucatán Peninsula, Mexico. *Geology* **19**, 867–871 (1991).

- Brownlee, D. E. Cosmic dust: collection and research. *Annu. Rev. Earth Planet. Sci.* **13**, 147–173 (1985).
- Pierazzo, E., Kring, D. A. & Melosh, H. J. Hydrocode simulation of the Chicxulub impact event and the production of climatically active gases. *J. Geophys. Res. E* (submitted).
- Rea, D. K., Leinen, M. & Janecek, T. R. Geologic approach to the long-term history of atmospheric circulation. *Science* **227**, 721–725 (1985).
- Kyte, F. T., Bostwick, J. A. & Zhou, L. The Cretaceous-Tertiary boundary on the Pacific plate: composition and distribution of impact debris. *Geol. Soc. Am. Spec. Pap.* **307**, 389–401 (1996).
- Kyte, F. T., Bostwick, J. A. & Zhou, L. Identification of the Cretaceous-Tertiary boundary at ODP Site 886, ODP Site 803, and DSDP Site 576. *Proc. ODP Sci. Res.* **145**, 427–434 (1995).
- Bostwick, J. A. & Kyte, F. T. The size and abundance of shocked quartz in Cretaceous-Tertiary boundary sediments from the Pacific basin. *Geol. Soc. Am. Spec. Pap.* **307**, 403–415 (1996).
- Kyte, F. T. & Bostwick, J. A. Magnesian spinel in Cretaceous-Tertiary boundary sediments of the Pacific basin: Hot, early condensates of the Chicxulub impact? *Earth Planet. Sci. Lett.* **132**, 113–127 (1995).
- Thorslund, P. & Wickman, F. E. Middle Ordovician chondrite in fossiliferous limestone from Brunflo, central Sweden. *Nature* **289**, 285–286 (1981).
- Thorslund, P., Wickman, F. E. & Nystrom, J. A. The Ordovician chondrite from Brunflo, central Sweden. I. General description and primary minerals. *Lithos* **17**, 87–100 (1984).
- Blanchard, M. B., Brownlee, D. E., Bunch, T. E., Hodge, P. W. & Kyte, F. T. Meteoroid ablation spheres from deep-sea sediments. *Earth Planet. Sci. Lett.* **46**, 178–190 (1980).
- Zolensky, M., Barrett, R. & Browning, L. Mineralogy and composition of matrix and chondrule rims in carbonaceous chondrites. *Geochim. Cosmochim. Acta* **57**, 3123–3148 (1993).
- Kellemeyn, G. W., Rubin, A. E. & Wasson, J. T. The compositional classification of chondrites: V. The Karronda (CK) group of carbonaceous chondrites. *Geochim. Cosmochim. Acta* **55**, 893–904 (1991).
- Lynne, E. C. & Bonatti, D. Mobility of manganese in diagenesis of deep-sea sediments. *Mar. Geol.* **3**, 457–474 (1965).
- Deer, W. A., Howie, R. A. & Zussman, J. *An Introduction to the Rock-forming Minerals* 2nd edn (Wiley, New York, 1992).
- Love, S. G. & Brownlee, D. E. A direct measurement of the terrestrial mass accretion rate of cosmic dust. *Science* **262**, 550–553 (1993).
- Hut, P. *et al.* Comet showers as a cause of mass extinctions. *Nature* **329**, 118–126 (1987).
- Schultze, P. H. & Gault, D. E. Prolonged global catastrophes from oblique impacts. *Geol. Soc. Am. Spec. Pap.* **247**, 239–262 (1990).
- Schultz, P. H. & D'Hondt, S. D. Cretaceous-Tertiary (Chicxulub) impact angle and its consequences. *Geology* **24**, 963–967 (1996).
- Gerosonde, R. *et al.* Geological record and reconstruction of the late Pliocene impact of the Eitanin asteroid in the Southern Ocean. *Nature* **390**, 357–363 (1997).
- Schuraytz, B. L. *et al.* Iridium metal in Chicxulub impact melt: forensic chemistry on the K-T smoking gun. *Science* **271**, 1573–1576 (1996).
- Robin, E., Froget, L., Jéhanno, C. & Rocchia, R. Evidence for a K/T impact event in the Pacific Ocean. *Nature* **363**, 615–617 (1993).
- McSween, H. Y. Jr Petrographic variations among carbonaceous chondrites of the Vigarano type. *Geochim. Cosmochim. Acta* **41**, 1777–1790 (1977).
- McSween, H. Y. Jr Carbonaceous chondrites of the Ormans type: a metamorphic sequence. *Geochim. Cosmochim. Acta* **41**, 477–491 (1977).
- Weisberg, M. K., Prinz, P., Clayton, R. N. & Mayeda, T. K. The CR (Renazzo-type) carbonaceous chondrite group and its implications. *Geochim. Cosmochim. Acta* **43**, 1761–1770 (1979).
- McSween, H. Y. Jr Alteration in CM carbonaceous chondrites inferred from modal and chemical variations in matrix. *Geochim. Cosmochim. Acta* **57**, 1567–1586 (1993).
- Grossman, J. N., Rubin, A. E., Nagahara, H. & King, E. A. in *Meteorites and the Early Solar System* (eds Kerridge, J. F. & Matthews, M. S.) 619–659 (Univ. Arizona Press, Tucson, 1994).
- Wasson, J. T. *Meteorites: their Record of Early Solar System History* (Freeman, New York, 1985).
- Engrand, C. & Maurette, M. Carbonaceous micrometeorites from Antarctica. *Meteoritics* **33**, 565–580 (1998).
- Kellemeyn, G. W. & Wasson, J. T. The compositional classification of chondrites-I. The carbonaceous chondrite groups. *Geochim. Cosmochim. Acta* **45**, 1217–1230 (1981).

**Acknowledgements.** This manuscript benefited significantly from discussions with A. E. Rubin and comments from H. McSween, E. Pierazzo and M. Grady. This work was supported by the Geology and Paleontology Program of the National Science Foundation. Curation of DSDP cores is supported by the NSF.

Correspondence and requests for materials should be addressed to the author (e-mail: kyte@igpp.ucla.edu).

## Coherent quantum control of two-photon transitions by a femtosecond laser pulse

Doron Meshulach & Yaron Silberberg

Department of Physics of Complex Systems, Weizmann Institute of Science, Rehovot 76100, Israel

Coherent quantum control<sup>1–3</sup> has attracted interest as a means to influence the outcome of a quantum-mechanical interaction. In principle, the quantum system can be steered towards a desired state by its interaction with light. For example, in photoinduced transitions between atomic energy levels, quantum interference effects can lead to enhancement or cancellation of the total transition probability. The interference depends on the spectral

phase distribution of the incident beam; as this phase distribution can be tuned, the outcome of the interaction can in principle be controlled. Here we demonstrate that a femtosecond laser pulse can be tailored, using ultrashort pulse-shaping<sup>4-7</sup> techniques, to control two-photon transitions in caesium. By varying the spectral phases of the pulse components, we observe the predicted cancellation of the transitions due to destructive quantum interference; the power spectrum and energy of these 'dark pulses' are unchanged. We also show that the pulse shape can be modified extensively without affecting the two-photon transition probability.

Although schemes of coherent control can involve continuous waves, many proposals have been made that involved ultrashort optical pulses. For example, coherent control of molecular systems with a sequence of short pulses could allow the selective manipulation of molecular structures<sup>8</sup>, including breaking specific bonds and changing a reaction path. Most of these schemes involve exciting the system with short pairs of pulses<sup>9-14</sup>. Such control by pulse pairs was also demonstrated for various one-photon<sup>15,16</sup> and two-photon transitions in two-level systems<sup>17-20</sup>.

Consider the two-photon interaction of an ultrashort pulse with a field  $e(t)$  with a two-level atom. If the interaction is non-resonant (that is, a transition with no intermediate states), the probability of inducing a transition to the excited state by the pulse is proportional to:

$$S_2 = \left| \int E(\omega_0/2 + \Omega)E(\omega_0/2 - \Omega)d\Omega \right|^2 = \left| \int A(\omega_0/2 + \Omega)A(\omega_0/2 - \Omega) \exp \left\{ i[\Phi(\omega_0/2 + \Omega) + \Phi(\omega_0/2 - \Omega)] \right\} d\Omega \right|^2 \quad (1)$$

where  $E(\omega) = A(\omega)\exp[i\Phi(\omega)]$  is the Fourier transform of  $e(t)$ , and  $A(\omega)$  and  $\Phi(\omega)$  are the spectral amplitude and the spectral phase distribution, respectively. Equation (1) reflects the fact that two-photon transitions occur for all pairs of photons with frequencies  $\omega_1, \omega_2$  (with  $\omega_1 + \omega_2 = \omega_0$ ), and  $\omega_1, \omega_2$  lie within the spectrum of the exciting pulse, as shown schematically in Fig. 1. Hence, all frequency components of a single pulse contribute to the two-photon transition probability, which can be controlled by tailoring the spectral phases of the pulse.

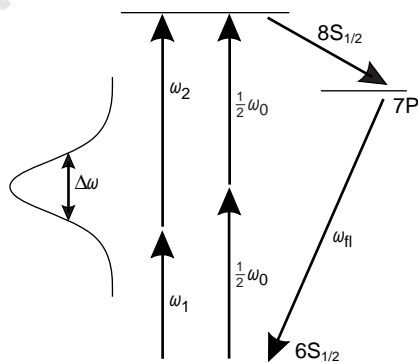


**Figure 1** Schematic diagram of the energy levels of the  $6S_{1/2} - 8S_{1/2}$  two-photon transitions in Cs. Two-photon transitions occur for all pairs of photons  $\omega_1, \omega_2$  (with  $\omega_1 + \omega_2 = \omega_0$ ), where  $\omega_0$ , which corresponds to 411 nm, is the energy of the transition. The fluorescence signal  $\omega_{fl}$  corresponds to  $\sim 460$  nm. The power spectrum of the excitation pulse is shown schematically at the left. Note that each of the two levels is split into two hyperfine states. Only two transitions are allowed, one from each of the sublevels of the ground state to the corresponding excited state. In our experiments, all signals were shorter than a few picoseconds, which is too short to observe any dynamics between the two transitions; we therefore consider the ground and excited states as single states.

For a given power spectrum  $A^2(\omega)$ , it is obvious that  $S_2$  is maximized by the transform limited pulse, that is, a pulse having the minimum time duration with  $\Phi(\omega) = 0$ . For a pulse with the same power spectrum, but having any antisymmetric spectral phase distribution around the two-photon transition frequency  $\omega_0/2$ , that is  $\Phi(\omega_0/2 + \Omega) = -\Phi(\omega_0/2 - \Omega)$ , the two-photon transition probability is independent of the spectral phase, and is identical to that of the transform limited pulse. But it is obvious that such an antisymmetric spectral phase affects the pulse shape. In fact, the pulse can be spread in time into a very small amplitude without affecting the two-photon transition probability.

Although antisymmetric phase distributions do not affect the two-photon transition probability, other phase distributions can be tailored to cancel the two-photon transition probability. Such so-called dark pulses, which could come in various temporal shapes, induce no net two-photon transitions, and are the appropriate coherent superposition of optical frequencies that cancels two-photon absorption. They are analogous to dark states, which are coherent superpositions of quantum states that do not absorb resonant light.

To verify our predictions experimentally, we considered the two-photon transitions between the  $6S_{1/2}$  and the  $8S_{1/2}$  levels of atomic caesium, induced by a femtosecond pulse as shown in Fig. 1, where  $\omega_0/2$  corresponds to 822 nm. Each of the excited atoms decays spontaneously to the ground level through the 7P level, so that the two-photon transition can be directly observed through the measurement of the two-photon fluorescence signal at  $\omega_{fl}$ , which corresponds to  $\sim 460$  nm.

The layout of our experimental system, shown in Fig. 2, is composed of a programmable pulse shaper, a Cs gas cell, a photomultiplier and a lock-in amplifier. We tuned our mode-locked Ti-sapphire laser, to produce 31-fs full-width at half-maximum (FWHM) transform-limited  $\text{sech}^2$  intensity pulses, centred at 822 nm, at the output of the pulse shaper. The programmable pulse shaper<sup>7</sup> was composed of a pair of diffraction gratings with

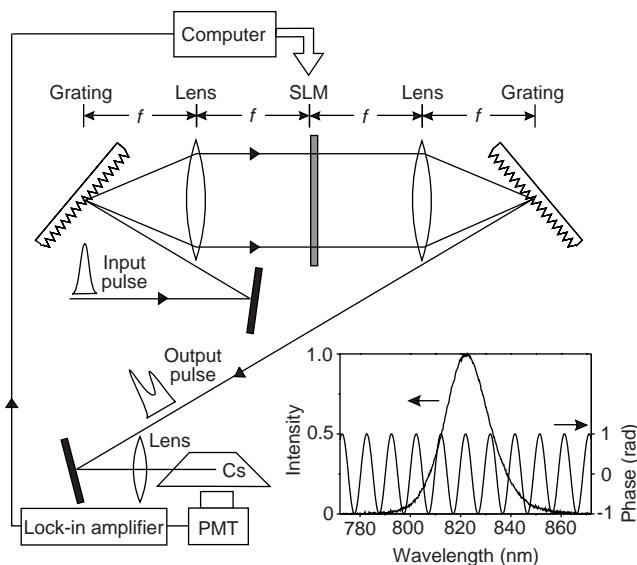


**Figure 2** Experimental system for coherent quantum control of two-photon transitions. The system is composed of a dynamic pulse shaper, a programmable liquid-crystal spatial light modulator used as a spatial filter, a Cs gas cell and a photomultiplier (PMT) and a lock-in amplifier. The computer was used for reading the fluorescence signal and for updating the modulator. The inset shows the normalized power spectrum of a typical input pulse with a FWHM of 23 nm, and a typical phase modulation with  $\Theta(\Omega) = \alpha \cos(\beta\Omega)$ ,  $\alpha = 1$  and  $\beta \approx 220$  fs. In all experiments, an additional constant-phase filter was applied to the modulator, to account for residual dispersion introduced by the pulse shaper, including that of the modulator itself.

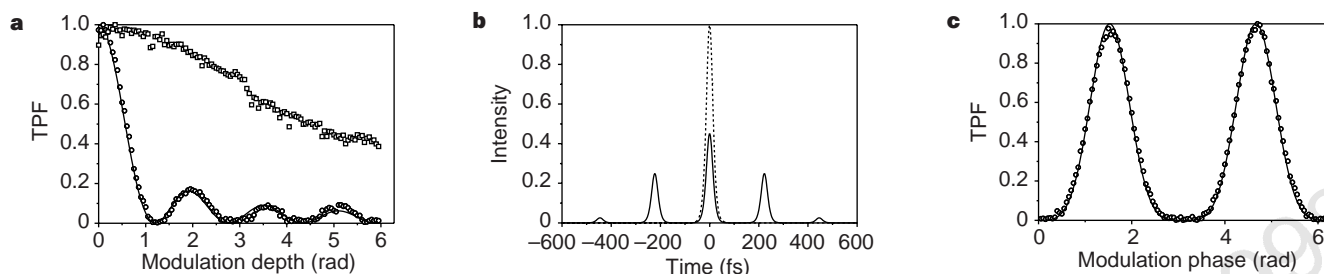


**Figure 3** Experimental and calculated results for coherent quantum control of two-photon transitions in Cs gas by a periodic phase distribution  $\Theta(\Omega) = \alpha \cos(\beta\Omega + \varphi)$ . In all cases,  $\beta \approx 220$  fs, which corresponds to about two periods of phase modulation within the FWHM spectral width of the pulses. **a**, Experimental (circles) and calculated (line) normalized two-photon fluorescence (TPF) signal as a function of the modulation depth  $\alpha$  for  $\varphi = 0$ . Also shown are experimental results (squares) for antisymmetric phase distribution  $\Theta(\Omega) = \alpha \sin(\beta\Omega)$ , as a

function of  $\alpha$ . **b**, The calculated normalized temporal intensity distribution of the dark pulse corresponding to  $\alpha = 1.2$  and  $\varphi = 0$  (solid line) and the transform-limited 31-fs  $\text{sech}^2$  intensity input pulse having the same power spectrum (dashed line). **c**, Experimental (circles) and calculated (line) fluorescence signal for phase distribution  $\Theta(\Omega) = \alpha \cos(\beta\Omega + \varphi)$  as a function of the modulation phase  $\varphi$  for  $\alpha = 1.2$ .

1,200 lines  $\text{mm}^{-1}$ , and a pair of achromatic lenses with a 100-mm focal length. Briefly, the first lens and grating spatially map the complex spectrum of the input pulse at the Fourier plane, where a spatial filter is inserted. The second lens and grating reassemble the spectral components to form a modified time-shaped pulse. A one-dimensional programmable liquid-crystal spatial light-modulator array, composed of 128 computer-controlled discrete phase elements was placed at the Fourier plane of the shaper, and was used as a dynamic filter for spectral phase manipulation of the pulses. The shaped output pulses were focused into the Cs gas cell, and the fluorescence signal was filtered optically and detected by the photomultiplier.

To demonstrate coherent control of the transition, we modified the phases of the spectral components of the input pulse by applying spectral phase-only filters of the form  $H(\Omega) = \exp(i\Theta(\Omega))$  to the modulator, where  $\Theta$  is the frequency deviation from  $\omega_0/2$ , and measured the fluorescence signal as a function of the parameters of the filters. Note that a phase-only filter does not affect the pulse energy or power spectrum. We limit the discussion here to periodic spectral phase distributions with  $\Theta(\Omega) = \alpha \cos(\beta\Omega + \varphi)$ , where  $\alpha$  and  $\beta$  are the modulation depth and frequency modulation, respectively, and  $\varphi$  is the modulation phase (see Fig. 2, inset, for a typical phase modulation). In all the experiments below,  $\beta \approx 220$  fs, which corresponds to about two periods of phase modulation over the spectral width of the pulses. The results seem not to be sensitive to this value.

First, we applied a symmetric spectral phase  $\Theta(\Omega) = \alpha \cos(\beta\Omega)$ , and measured the fluorescence signal as a function of the modulation depth  $\alpha$ . The experimental results are presented in Fig. 3a, together with the theoretical curve calculated from equation (1) with  $E(\omega_0/2 + \Omega) = \text{sech}(1.76\Omega/\Delta\omega) \exp[i\alpha \cos(\beta\Omega)]$ , where  $\Delta\omega$  is the FWHM bandwidth of the power spectrum. We note a strong variation in the fluorescence signal as  $\alpha$  is increased. The fluorescence vanishes at a few values of the modulation depth, the first is near  $\alpha = 1.2$ ; these are dark pulses that induce no two-photon transitions. The calculated temporal distribution of the first dark pulse is shown in Fig. 3b, together with the transform-limited input pulse having the same power spectrum. Because of the periodicity of the spectral phase, this dark pulse is a particular sequence of pulses. Other dark pulses are obtained for higher values of  $\alpha$ . The vanishing of the fluorescence signal near  $\alpha = 1.2$  is related to the first zero of the Bessel function  $J_0(2\alpha_0) = 0$ . For a square uniform spectrum of width  $\Delta\omega$  it can be shown analytically that  $S_2 = 0$  in equation (1) for  $\beta = 2\pi/\Delta\omega$  and  $\alpha_0 = 1.2024$ .

Also shown in Fig. 3a are experimental results with antisymmetric spectral phase  $\Theta(\omega) = \alpha \sin(\beta\Omega)$ . Although theory predicts a constant fluorescence signal, we measure a slow decrease in the signal with increasing  $\alpha$ . We attribute this discrepancy to inherent loss and

imperfect antisymmetry due to the use of discrete phase elements in the modulator. But note that for  $\alpha = 1.2$ , the fluorescence intensity drops only by a few per cent for this antisymmetric filter, whereas it vanishes for the symmetric filter. In the time domain, the corresponding fields differ only in their phase structure; that is, their intensities  $|e(t)|^2$  are practically identical. It is this phase structure that leads to the markedly different outcome of the quantum mechanical process. Antisymmetric phase modulation generates a sequence of pulses as in Fig. 3b that are all in a single quadrature of the field, whereas symmetric modulation generates pulses that alternate between the two quadratures. Pulses of different quadratures lead to destructive interference of the two-photon transition probability<sup>17–19</sup> and, at the appropriate ratio, to its complete cancellation.

To emphasize the importance of symmetry, we measured the fluorescence signal as a function of the modulation phase  $\varphi$  for  $\alpha = 1.2$ . This allows monitoring of the transition probability as the spectral phase distribution is continuously transformed from symmetric to antisymmetric. The experimental and theoretical results are presented in Fig. 3c. Note that simply by shifting the phase-modulation filter across the spectrum, affecting neither the total power nor the power spectrum of the pulse, we were able to control the fluorescence yield by a factor of better than 1 in 200. This is a very impressive demonstration of the effectiveness of quantum interference to achieve coherent control of a quantum-mechanical process. Note also that all theoretical and experimental results are presented without adjustable parameters. The excellent agreement between the experimental results and the simple theory outlined above reflects the fundamental role of quantum interference in two-photon absorption.

Although we could demonstrate remarkable agreement between theory and experiment for a two-level system, two-photon processes in molecular and other complex quantum systems are usually too complicated to model exactly. Nevertheless, we expect that coherent control in such complex systems can be achieved by introducing adaptive ultrashort-pulse-manipulation techniques<sup>3,21–25</sup> that optimize the spectral phases to approach a goal without any prior knowledge of the system.

The principles presented here can be extended straightforwardly to many other multiphoton interactions of ultrashort pulses with matter, including Raman transitions, and work in this direction is in progress. We expect that these findings will open a wide new area for theoretical and experimental work, as well as possible applications in nonlinear spectroscopy and in atomic and molecular physics. □

Received 29 June; accepted 18 August 1998.

- Rice, S. A. New ideas for guiding the evolution of a quantum system. *Science* **258**, 412–413 (1992).
- Brumer, P. & Shapiro, M. Laser control of chemical reactions. *Sci. Am.* **272**(3), 34–39 (1995).

- Warren, W. S., Rabitz, H. & Dahleh, M. Coherent control of quantum dynamics: the dream is alive. *Science* **259**, 1581–1589 (1995).
- Weiner, A. M. & Heritage, J. P. Picosecond and femtosecond Fourier pulse shape synthesis. *Rev. Phys. Appl.* **22**, 1619–1628 (1987).
- Weiner, A. M., Leaird, D. E., Patel, J. S. & Wullert, J. R. Programmable femtosecond pulse shaping by use of a multielement liquid-crystal phase modulator. *Opt. Lett.* **15**, 326–328 (1990).
- Hillegas, C. W., Tull, J. X., Goswami, D., Strickland, D. & Warren, W. S. Femtosecond laser pulse shaping by use of microsecond radio-frequency pulses. *Opt. Lett.* **19**, 737–739 (1994).
- Wefers, M. M. & Nelson, K. A. Generation of high-fidelity programmable ultrafast optical waveforms. *Opt. Lett.* **20**, 1047–1049 (1995).
- Tannor, D. J. in *Molecules in Laser Fields* (ed. Bandrauk, A.) 403–446 (Dekker, New York, 1994).
- Tannor, D. J. & Rice, S. A. Control of selectivity of chemical reaction via control of wave packet evolution. *J. Chem. Phys.* **83**, 5013–5018 (1985).
- Tannor, D. J., Kosloff, R. & Rice, S. A. Coherent pulse sequence induced control of selectivity of reactions: exact quantum mechanical calculations. *J. Chem. Phys.* **85**, 5805–5820 (1986).
- Shapiro, M. & Brumer, P. Laser control of product quantum state populations in unimolecular reactions. *J. Chem. Phys.* **84**, 4103–4104 (1986).
- Tannor, D. J. & Rice, S. A. Coherence pulse sequence control of product formation in chemical reactions. *Adv. Chem. Phys.* **70**, 441–523 (1988).
- Brumer, P. & Shapiro, M. Laser control of molecular processes. *Annu. Rev. Phys. Chem.* **43**, 257–282 (1992).
- Potter, E., Herek, J. L., Pedersen, S., Liu, Q. & Zewail, A. H. Femtosecond laser control of a chemical reaction. *Nature* **355**, 66–68 (1992).
- Fourkas, J. T., Wilson, W. L., Wäckerle, G., Frost, A. E. & Fayer, M. D. Picosecond time-scale phase-related optical pulses: measurement of sodium optical coherence decay by observation of incoherent fluorescence. *J. Opt. Soc. Am. B* **6**, 1905–1910 (1989).
- Heberle, A. P., Baumberg, J. J. & Köhler, K. Ultrafast coherent control and destruction of excitations in quantum wells. *Phys. Rev. Lett.* **75**, 2598–2601 (1995).
- Salour, M. M. & Cohen-Tannoudji, C. Observation of Ramsey's interference fringes in the profile of doppler-free two-photon resonances. *Phys. Rev. Lett.* **38**, 757–760 (1977).
- Teets, R., Eckstein, J. & Häscher, T. W. Coherent two-photon excitation by multiple light pulses. *Phys. Rev. Lett.* **38**, 760–764 (1977).
- Blanchet, V., Nicole, C., Bouchene, M. & Girard, B. Temporal coherent control in two-photon transitions: from optical interferences to quantum interferences. *Phys. Rev. Lett.* **78**, 2716–2719 (1997).
- Bellini, M., Bartoli, A. & Häscher, T. W. Two-photon Fourier spectroscopy with femtosecond light pulses. *Opt. Lett.* **22**, 540–542 (1997).
- Judson, R. S. & Rabitz, H. Teaching lasers to control molecules. *Phys. Rev. Lett.* **68**, 1500–1503 (1992).
- Meshulach, D., Yelin, D. & Silberberg, Y. Adaptive ultrashort pulse compression and shaping. *Opt. Commun.* **138**, 345–348 (1997).
- Yelin, D., Meshulach, D. & Silberberg, Y. Adaptive femtosecond pulse compression. *Opt. Lett.* **22**, 1793–1795 (1997).
- Meshulach, D., Yelin, D. & Silberberg, Y. Adaptive real-time femtosecond pulse shaping. *J. Opt. Soc. Am. B* **15**, 1615–1619 (1998).
- Bardeen, C. J. *et al.* Feedback quantum control of molecular electronic population transfer. *Chem. Phys. Lett.* **280**, 151–158 (1997).

**Acknowledgements.** We thank C. Cohen-Tannoudji, N. Davidson, T. W. Hänsch and D. Tannor for helpful discussions, D. Yelin for his help in developing pulse-shaping techniques and A. Arie for loan of the Cs cell.

Correspondence and requests for materials should be addressed to Y.S. (e-mail: feyaron@wis.weizmann.ac.il).

## Observation of a square flux-line lattice in the unconventional superconductor $\text{Sr}_2\text{RuO}_4$

T. M. Riseman\*, P. G. Kealey\*, E. M. Forgan\*, A. P. Mackenzie\*, L. M. Galvin\*, A. W. Tyler\*, S. L. Lee†, C. Ager†, D. McK. Paul‡, C. M. Aegerter§, R. Cubitt||, Z. Q. Mao¶, T. Akima¶ & Y. Maeno¶

\* School of Physics and Astronomy, University of Birmingham, Birmingham B15 2TT, UK

† School of Physics and Astronomy, University of St Andrews, St Andrews KY16 9SS, UK

‡ Department of Physics, University of Warwick, Coventry CV4 7AL, UK

§ Physik-Institut der Universität Zürich, CH-8057, Zurich, Switzerland

|| Institut Laue-Langevin, F-38042, Grenoble, France

¶ Department of Physics, Kyoto University, Kyoto 606-8052, Japan

The phenomenon of superconductivity continues to be of considerable scientific and practical interest. Underlying this phenomenon is the formation of electron pairs, which in conventional superconductors do not rotate about their centre of mass ('s-wave' pairing; refs 1, 2). This contrasts with the

situation in high-temperature superconductors, where the electrons in a pair are believed to have two units of relative angular momentum ('d-wave' pairing; ref. 3 and references therein). Here we report small-angle neutron-scattering measurements of magnetic flux lines in the perovskite superconductor  $\text{Sr}_2\text{RuO}_4$  (ref. 4), which is a candidate for another unconventional paired electron state—'p-wave' pairing, which has one unit of angular momentum<sup>5–7</sup>. We find that the magnetic flux lines form a square lattice over a wide range of fields and temperatures, which is the result predicted by a recent theory<sup>8,9</sup> of p-wave superconductivity in  $\text{Sr}_2\text{RuO}_4$ . This theory also indicates that only a fraction of the electrons are strongly paired and that the orientation of the square flux lattice relative to the crystal lattice will determine which parts of the three-sheet Fermi surface of this material are responsible for superconductivity. Our results suggest that superconductivity resides mainly on the 'γ' sheet<sup>9</sup>.

Strontium ruthenate (SRO) has nearly two-dimensional metallic properties, with a well-established Fermi surface<sup>10–13</sup> consisting of three sheets (α, β, γ). Non-s-wave superconductivity in this material is implied by the strong suppression of the superconducting transition temperature ( $T_c$ ) below its maximum value of ~1.5 K by non-magnetic impurities, which thus act as pair-breakers<sup>7</sup>. Noting that the γ-sheet of the SRO Fermi surface is mainly derived from different Ru orbitals than are the α- and β-sheets, Agerter *et al.*<sup>8</sup> have argued that pairing interactions will only weakly couple the different orbitals. They propose that p-wave superconductivity will be primarily present on either the γ-sheet, or the α- and β-sheets, with weak superconductivity on the other. This argument has been recently extended by Agerter<sup>9</sup>, who has shown that the flux-line lattice (FLL) structure for field perpendicular to the  $\text{RuO}_2$  planes is very likely to be square, and that the orientation of the square flux lattice relative to the crystal lattice indicates which sheet(s) of the Fermi surface are primarily responsible for superconductivity. Thus, by observations of the flux lattice, we can gain important information about superconductivity in this material.

Neutron-diffraction patterns were obtained from the FLL in a sample of SRO (see Methods). A contour plot of a typical result is

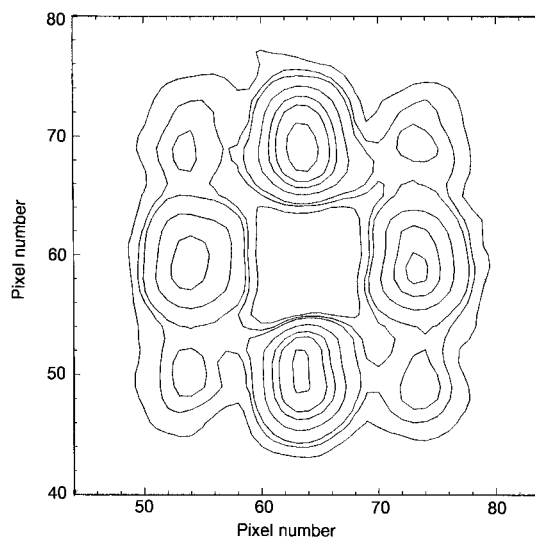


**Figure 1** Contour plot of FLL diffraction pattern. With the geometry of our experiments, the diffracted neutrons form an image in the multidetector of the reciprocal lattice of the FLL: the central region of the detector has been masked. A field of 20 mT was applied parallel to **c** above  $T_c$ ; data taken above  $T_c$  were subtracted from that obtained after cooling to 100 mK. The crystal **a** and **b** directions are horizontal and vertical in this figure. The sample shape causes the vertical spots to have different intensities from the horizontal ones, as discussed in Methods. The elongated shape of the spots reflects the shape of the exit aperture of the neutron guide.